Proceedings of the ASME International Mechanical Engineering Congress & Exposition
IMECE09
November 13-19, 2009, Lake Buena Vista, Florida, USA

IMECE2009-11527

DIRECT NUMERICAL SIMULATIONS OF MAGNETIC FIELD EFFECTS ON TURBULENT DUCT FLOWS

R. Chaudhary
Department of Mechanical Science & Engineering
University of Illinois at Urbana-Champaign
Urbana, IL, USA

S. P. Vanka
Department of Mechanical Science & Engineering
University of Illinois at Urbana-Champaign
Urbana, IL, USA

B. G. Thomas
Department of Mechanical Science & Engineering
University of Illinois at Urbana-Champaign
Urbana, IL, USA

ABSTRACT

Magnetic fields are crucial in controlling flow in various physical processes of significance. Magnetic fields are frequently used to pump, stir and stabilize liquid metal flows non-intrusively. One of these processes, which has significant application of a magnetic field, is continuous casting of steel, where different magnetic field configurations are used to control the turbulent steel flow in the mold to minimize defects in the cast steel. Recently, liquid metal MHD flows have been extensively studied for application to fusion reactor technology. This study has been undertaken to analyze the effect of magnetic field on mean velocities and turbulence parameters in the molten metal flows through a square duct. Direct Numerical Simulations without using a sub-grid scale (SGS) model have been used to characterize the three-dimensional transient flow. The coupled Navier-Stokes-MHD equations have been solved with a three-dimensional fractional-step numerical procedure. Convection as well as diffusion terms have been discretized using a central differencing scheme in space and the 2nd order Adams-Bashforth scheme for integration in time. Pressure-velocity coupling has been resolved using the fractional-step method and the pressure Poisson equation has been solved using a multigrid solver. Because liquid metals have low magnetic Reynolds number, the induced magnetic field has been neglected and the electric potential method for magnetic field-flow coupling has been implemented. The equation for electric potential has been also been calculated using a multigrid solver. The known electric potential and velocities then provide the current density which is used in the expression for Lorentz force in the momentum equations. Initially, laminar simulations in a square duct have been performed and results generated were compared with previous series solutions. Next, simulations of a non-MHD flow in a square duct at low Reynolds number were performed and satisfactorily compared with results of a previous DNS study. Subsequently, different levels of a magnetic field were applied to study its effect on the turbulence until the flow completely laminarized. Time-dependent and time-averaged flows have been studied through mean velocities and fluctuations, and power spectrums of instantaneous velocities.

INTRODUCTION

Magnetic fields are effective in controlling flow in various physical processes of significance such as metal processing, MHD pumps, flow meters, plasma and fusion technology, to name a few (1). One such process is continuous casting of steel in which different magnetic field configurations are used to control the turbulent flow of steel in the mold to minimize defects in cast steel (2). When a magnetic field is applied to a flow field, the interaction of the current density with the magnetic field generates a Lorentz force, which then brakes the flow and alters the velocity field (3). In the case of turbulent flows, magnetic fields can relaminarize the flow and alter significantly the structure of the turbulent flow (4). Consequently the friction characteristics and mixing phenomena in turbulent flows subjected to magnetic fields can be significantly different from those without the magnetic field. Tailoring the magnetic field to alter the flow in the mold of the continuous caster of steel is a topic of significant practical interest (2).

The common methodology used in many previous studies to simulate effects of magnetic field on turbulent flows has been the Reynolds-averaged approach (4-8). However, the

fundamental difficulty with such an approach is the modeling of the terms that alter the turbulent fluctuations due to the Lorentz forces (4). Specifically, it is difficult to predict the suppression of turbulence and modification of the flow structures through the time-averaged approach (4). Since the magnetic fields directly act on the turbulent fluctuations, a more rigorous method with solution of equations for the time-dependent three-dimensional turbulent flow is required. Recently, with the significant improvement in computer speed, Direct Numerical Simulation (DNS) has gained importance as a complementary tool to experiments (9). In the present work, we have studied using DNS the effects of magnetic field on flow through a square duct.

Extensive studies exist on turbulence in channel flows using DNS, Large Eddy Simulations and experiments (e.g. Kim, Moin and Moser , Spalart, Moser and Moin (10-12)). Relatively, a fewer number of studies have considered flow in a square duct in which two inhomogeneous directions exist (13-15). The first DNS with two inhomogeneous directions was performed by Gavrilakis (13). Standard finite difference scheme with 16 million nodes and a moderate Reynolds number of 4410 were used. The turbulence-driven secondary flows were accurately predicted. Turbulent statistics showed good agreement with the channel data at the wall bisectors, including bulging of streamwise mean flow profile. Huser and Biringen (1993) used a time-splitting method with spectral/higher-order finite difference discretization on a staggered mesh to simulate turbulent square duct flow (14). In their study, the Reynolds number based upon friction velocity was taken to be 600 and 96x101x101 grid points were used. Madabhushi and Vanka (1991, 1993) performed LES and DNS in a straight square duct using a mixed spectral-finite difference method (15-16). DNS at Re_τ of 260 and LES at 360 were found to predict secondary flows and turbulence statistics correctly.

Only a few previous studies are available of DNS of turbulent flow subjected to a magnetic field (17-21). Satake, Kunugi and Smolentsev (2002) performed DNS to investigate turbulent pipe flow in a transverse magnetic field at a moderate Reynolds number of 5300 and three Hartmann numbers of 5, 10, and 20 (17). The skin friction, velocity profiles, turbulent intensities and turbulent kinetic energy budget were studied along the circumferential direction of the pipe. At horizontal locations close to wall, velocity profile was observed to become more rounded with Hartmann flattening seen at the top of the pipe. Lee and Choi (2001) performed DNS of flow in a channel to study the effect of magnetic field orientation on the pressure drop (18). They considered streamwise, wall-normal and spanwise magnetic fields and found increase in drag due to Hartmann effect in the wall normal magnetic field case. Satake, Kunugi, Takase and Ose (2006) studied the effect of magnetic field on wall bounded turbulence in a channel using DNS at a high Re of 45818 and Hartmann numbers of 32.5 and 65 (19). A uniform magnetic field was applied normal to the wall and various turbulent quantities were analyzed. Large scale structures were found to decrease in the core of the channel. Therefore, the difference between production and dissipation in the turbulent kinetic energy was found to be decreasing upon increasing Hartmann number in the central region of the channel.

Zikanov and Thess (1998, 2004) studied the effect of magnetic field on the turbulence using DNS in a classical 3-D cube with all directions having periodic boundary conditions (20-21). Dependence of turbulence was studied on magnetic interaction parameter (called Stuart number). At a low Stuart number, turbulence was found to be three-dimensional and approximately isotropic while turbulence suppression was seen at large Stuart numbers (strong magnetic field).

Kobayashi (2008) performed LES on a square duct with transverse magnetic field for Re=5300 and Re=29000 with 64x64x64 and 128x128x128 grids respectively (22). At Re=5300, Hartmann layer as well as side-wall layers were found laminarizing together at nearly the same Hartmann number. At higher Reynolds number (Re=29000), the top and bottom Hartmann layers laminarized first, followed by the side-wall layers.

In the present work, we have conducted DNS of turbulent flow in a square duct subjected to a progressively increasing Hartmann number. The flow structures and mean velocities are studied for a Reynolds number around 5000. The computer code was initially validated for laminar flow in a square duct with a transverse magnetic field and results thus generated were compared with previously known series solutions. Subsequently, simulations of flow in a square duct for a Reynolds number of 5500 have been performed without applying a magnetic field and results were compared with previous work of Gavrilakis (1992).Afterwards, a magnetic field was applied in the vertical direction and computations with 64x64x128 and 80x80x256 cells were performed. Mean and RMS velocities, and power spectrums have been collected and analyzed. The effect of magnetic field on friction losses in the duct is also evaluated.

NOMENCLATURE

$\vec{v}\,(u,v,w)$: velocity vector (x-, y- and z- components).

$u_\tau = \sqrt{\tau_w / \rho}$: friction velocity

p : Pressure

μ , ν : Dynamic and kinematic viscosities

$\vec{F}_L$: Lorentz force vector

ρ : Density

x , y , z : x-, y- and z- coordinates

Re_m: Magnetic Reynolds number

$\vec{J}$ (J_x, J_y, J_z):Current density (x-, y- and z- components)

$\vec{B}_0$: Externally applied magnetic field vector

ϕ : Electric potential

D_h : Hydraulic diameter

σ : Electrical conductivity

Re : Reynolds number

Ha : Hartmann number

$y^+ = yu_\tau / \nu$: normalized wall distance

N : Magnetic interaction parameter

Superscript: n : nth time level

GOVERNING EQUATIONS FOR A MAGNETOHYDRODYNAMIC FLOW

It is well-known that when an electrically conducting material moves through a magnetic field, an electric current is induced. This induced electric current interacts with the magnetic field and produces a force (J x B) on the flow field, called the Lorentz force. This Lorentz force brakes the flow and therefore opposes the very mechanism that created it. The following equations mathematically describe the flow evolution for an incompressible flow (23).

Continuity equation:

$$\nabla \cdot \vec{v} = 0 \tag{1}$$

Momentum equations (x-, y- and z-)

$$\rho\left(\frac{\partial \vec{v}}{\partial t} + \nabla \cdot (\vec{v}\vec{v})\right) = -\nabla p + \nabla \cdot \mu \nabla \vec{v} + \vec{F}_L \tag{2}$$

Since magnetic Reynolds number (Re_m) is < 1 in liquid metals, induced magnetic field because of the induced electric current can be neglected. After neglecting the induced magnetic field, the electric potential method can be used to determine the current and the Lorentz force by the following equations (3).

$$\vec{F}_L = \vec{J} \times \vec{B}_0 \tag{3}$$

$$\vec{J} = \sigma\left(-\nabla\phi + \vec{v} \times \vec{B}_0\right) \tag{4}$$

$$\nabla \cdot \vec{J} = 0 \tag{5}$$

By inserting current from Eq.(4) into the conservation of charge Eq.(5), Poisson's equation for electric potential can be derived, given as

$$\nabla^2 \phi = \nabla \cdot \left(\vec{v} \times \vec{B}_0\right) \tag{6}$$

There are essentially two non-dimensional parameters that govern the flow field. They are the Reynolds and Hartmann numbers which are defined as,

$$\mathrm{Re} = \frac{D_h u_m}{\nu} \qquad Ha = D_h B_0 \sqrt{\frac{\sigma}{\rho \nu}}$$

where, D_h is the hydraulic diameter, B_0 is the applied magnetic field, ν is kinematic viscosity, ρ is density and σ is the electrical conductivity of the fluid.

PHYSICAL DOMAIN AND BOUNDARY CONDITIONS

The physical and computational domains considered in this study are shown in Fig. 1. Two directions of the domain are bounded by walls, whereas the main flow direction is considered to be periodic. A constant and uniform magnetic field is applied in the vertical (y) direction. The size of the domain is 1 unit in the x and y directions and 2π in the z direction. This is discretized with 32x32x64, 64x64x128 and 80x80x256 cells for the different cases studied. No-slip and insulated wall boundary conditions have been used for the sides and top and bottom walls. Thus,

$\vec{v} = 0$, $J_y = 0 \Rightarrow \dfrac{\partial \phi}{\partial y} = 0$ at top and bottom walls

$\vec{v} = 0$, $J_x = 0 \Rightarrow \dfrac{\partial \phi}{\partial x} = 0$ at side walls

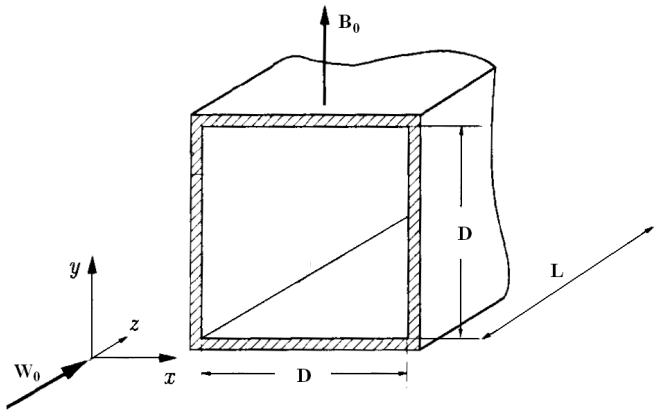

Fig. 1 Physical and computational domain

NUMERICAL METHOD

The three-dimensional coupled equations have been discretized using the finite volume method. Pressure-velocity coupling has been resolved through the fraction step method (24) with explicit formulation of diffusion and convection in the momentum equations. The method consists of the following steps.

x-momentum equation:

$$\left(H_u\right)^n = \left(-u\frac{\partial u}{\partial x} - v\frac{\partial u}{\partial y} - w\frac{\partial u}{\partial z} + \nu\left(\frac{\partial^2 u}{\partial x^2} + \frac{\partial^2 u}{\partial y^2} + \frac{\partial^2 u}{\partial z^2}\right)\right)^n$$

$$\left(\frac{u^{n+1} - u^n}{\Delta t}\right) = \left(H_u\right)^n - \frac{1}{\rho}\left(\frac{\partial p}{\partial x}\right)^{n+1} \tag{7}$$

y-momentum equation:

$$(H_v)^n = \left(-u\frac{\partial v}{\partial x} - v\frac{\partial v}{\partial y} - w\frac{\partial v}{\partial z} + \nu\left(\frac{\partial^2 v}{\partial x^2} + \frac{\partial^2 v}{\partial y^2} + \frac{\partial^2 v}{\partial z^2}\right)\right)^n$$

$$\left(\frac{v^{n+1} - v^n}{\Delta t}\right) = (H_v)^n - \frac{1}{\rho}\left(\frac{\partial p}{\partial y}\right)^{n+1} \quad (8)$$

z-momentum equation:

$$(H_w)^n = \left(-u\frac{\partial w}{\partial x} - v\frac{\partial w}{\partial y} - w\frac{\partial w}{\partial z} + \nu\left(\frac{\partial^2 w}{\partial x^2} + \frac{\partial^2 w}{\partial y^2} + \frac{\partial^2 w}{\partial z^2}\right)\right)^n$$

$$\left(\frac{w^{n+1} - w^n}{\Delta t}\right) = (H_w)^n - \frac{1}{\rho}\left(\frac{\partial p}{\partial z}\right)^{n+1} \quad (9)$$

$$\left(\frac{\partial}{\partial x}\left(\frac{\partial p}{\partial x}\right)^{n+1} + \frac{\partial}{\partial y}\left(\frac{\partial p}{\partial y}\right)^{n+1} + \frac{\partial}{\partial z}\left(\frac{\partial p}{\partial z}\right)^{n+1}\right) = \frac{\rho}{\Delta t}\left(\frac{\partial (u^*)^{n+1}}{\partial x} + \frac{\partial (v^*)^{n+1}}{\partial y} + \frac{\partial (w^*)^{n+1}}{\partial z}\right) \quad (10)$$

$$u^{n+1} = (u^*)^{n+1} - \frac{\Delta t}{\rho}\left(\frac{\partial p}{\partial x}\right)^{n+1} \quad (11)$$

$$v^{n+1} = (v^*)^{n+1} - \frac{\Delta t}{\rho}\left(\frac{\partial p}{\partial y}\right)^{n+1} \quad (12)$$

$$w^{n+1} = (w^*)^{n+1} - \frac{\Delta t}{\rho}\left(\frac{\partial p}{\partial z}\right)^{n+1} \quad (13)$$

Convection and diffusion terms have been discretized using second order central differencing scheme in space. Time integration has been achieved using explicit second order Adams-Bashforth scheme. A multigrid solver has been used to solve for pressure Poisson's equation.

With known velocity and pressure fields, the Poisson's equation for electric potential is solved for ϕ using a multigrid solver. The Lorentz force is then calculated and added as a source term in momentum equations for next time step.

RESULT AND DISCUSSION

We now present the results of various calculations performed in this study. First, we compared our results for a zero Hartmann number with those of Gavrilakis (13). Fig. 2(a) and (b) shows a snapshot of the instantaneous and mean flow field, shown as contours of the streamwise velocity and vectors of the cross-sectional velocities. Also shown is an instantaneous picture of the flow at a y+ of 8.85 in Fig. 2(c). Regions of high and low speed streaks are clearly visible at the plane signifying the near wall structures.

Fig. 3(a) shows a comparison of the normalized axial velocity with results of Gavrilakis (1992) (13) at Re=4410. Mean axial velocity along horizontal bi-sector of the current simulation is found to match well in the core but small differences are observed close to wall which may be due to the slightly different Reynolds numbers. Fig. 3(b) shows the comparison of axial velocity normalized with friction velocity along diagonal of the duct with Gavrilakis (1992) (13). The slight mismatch in the core can be mainly attributed to the difference in the friction velocity due to different Reynolds numbers.

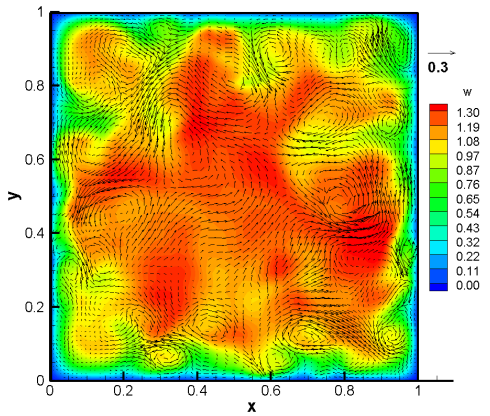

Fig. 2(a) Instantaneous axial velocity contours with secondary velocity vectors

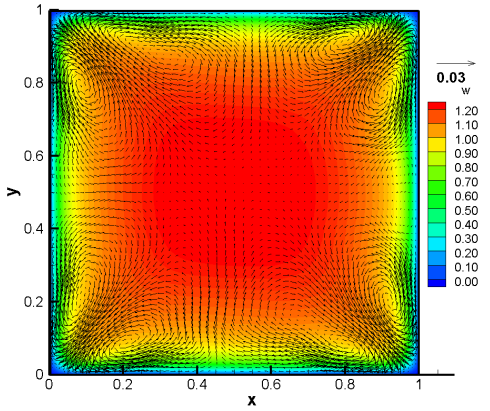

Fig. 2(b) Mean axial velocity contours with secondary velocity vectors

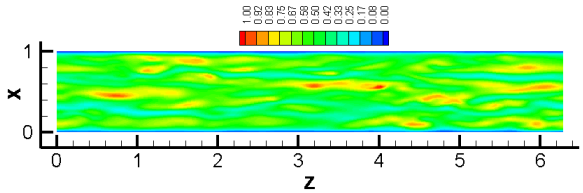

Fig. 2(c) Instantaneous velocity contours at y^+=8.85

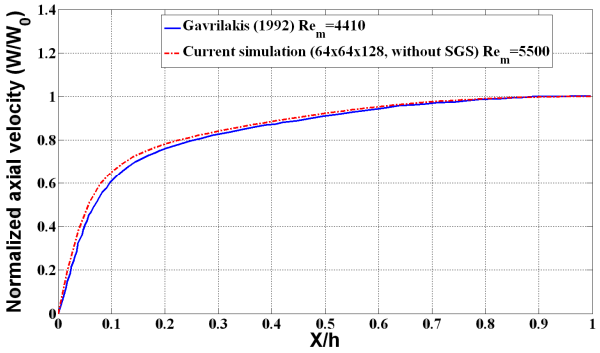

Fig. 3(a) Mean velocity comparison along horizontal bisector with Gavrilakis (13)

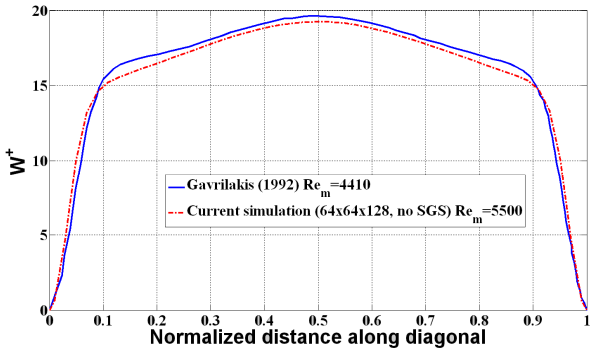

Fig. 3(b) Mean velocity comparison along diagonal with Gavrilakis (13)

Results with the magnetic field

Fig. 4 shows comparisons of the normalized axial velocity with analytical series solution of Muller and Buhler (25) for a laminarized square duct flow with transverse magnetic field. Here the flow was initiated with a dp/dz corresponding to Re=5500 and a perturbation (1% of the mean) in three velocities was applied for the initial 1500 timesteps to initiate turbulence. A strong magnetic field corresponding to Ha=60 was applied. The strong magnetic field was found to damp turbulence with flattening of velocity close to top and bottom walls. Axial velocity close to side-walls is found to agree with the laminar profile.

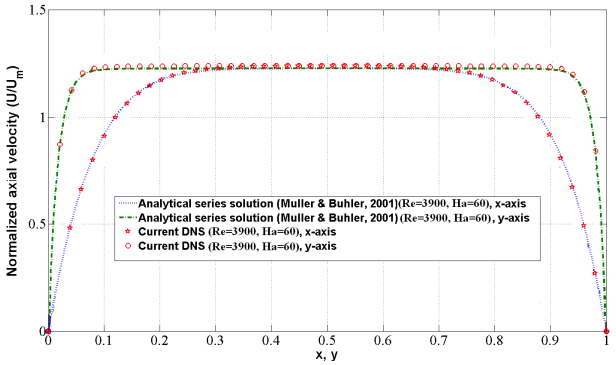

Fig.4 Comparison of laminarized solution with Muller & Buhler (15) with a (64x64x128) grid

Fig.5(a) shows normalized mean axial velocity along horizontal bisector for various Hartmann numbers. A constant mean pressure gradient corresponding to Re = 5300 at zero Hartmann number was applied for all cases. The Reynolds number therefore varied based on the magnetic braking and the velocity gradients. It can be seen that at Ha=21.2, Reynolds number increased from Re=5300 to 5978. This initially appears counter intuitive because rather than providing more resistance to the flow the magnetic field is seen to assist the flow. However, by suppressing the turbulence the wall friction can decrease and thereby the Reynolds number can increase. In Fig. 5, the current results (which give a Re of 5978 for Ha = 21.2) are compared with results of Kobayashi (22). Also compared are results for Re = 5457 obtained by a coarser grid. Fig-5(b) compares normalized axial velocity along vertical bisector for various Hartmann numbers. The agreement with results of Kobayashi (22) for Ha = 21.2 is good. Upon further increasing the Hartmann number, velocity flattening takes over the turbulence suppression and velocity starts increasing close to wall and decreasing in central region (i.e. flattening effect close to side wall and in the central region). Upon further increase in the Hartmann number, the velocity profiles close to top-bottom and side-walls continue to flatten and thus lead to higher velocity gradients and frictional losses.

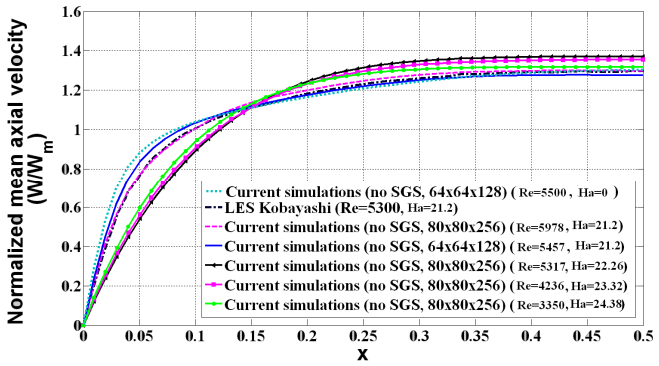

Fig-5(a) Mean axial velocity along horizontal bisectors in various cases

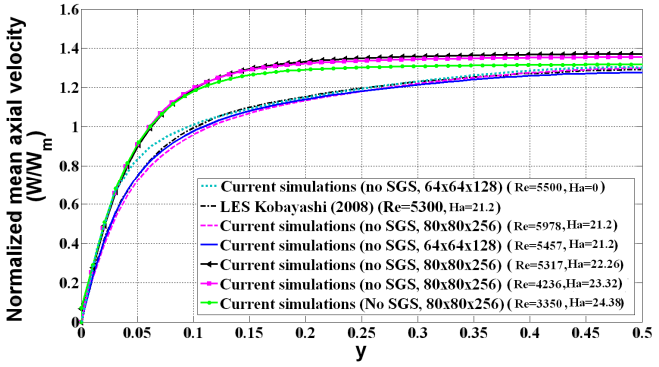

Fig-5(b) Mean axial velocity along vertical bisectors in various cases

Fig. 6(a) and (b) shows the instantaneous and mean velocities at a mid-axial direction cross-section for Re=5978 and Ha=21.2 case. It can be seen that the secondary flows are significantly modified in the presence of the magnetic field. Instead of going into the corners and causing higher axial velocity in the corners, the secondary flows are directed more towards the top and bottom walls and therefore causing the axial velocity profile to be slightly lifted towards top and bottom. Because of above behavior, reverse secondary velocities (i.e. from wall towards center) are at the centers of top and bottom walls, thus causing greater bulging in axial velocity at these locations. Fig-6(c) gives the axial velocity contours plotted at a plane at y^+=8.85.

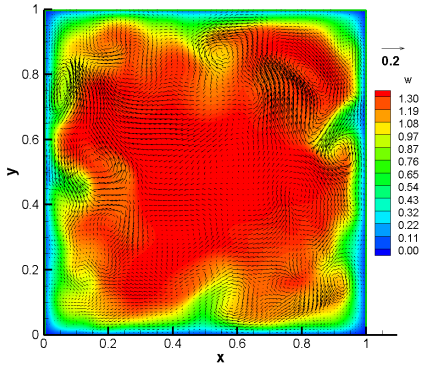

(Re=5978, Ha=21.2, 80x80x256)

Fig. 6(a) Instantaneous axial velocity contours with secondary velocity vectors

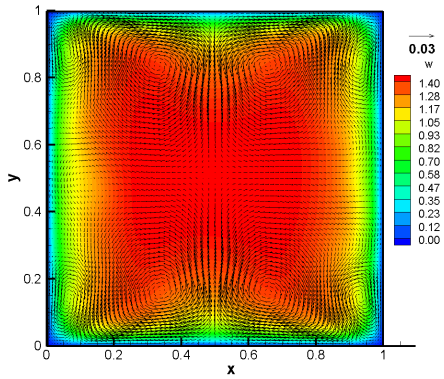

(Re=5978, Ha=21.2, 80x80x256)

Fig. 6(b) Mean axial velocity contours with secondary velocity vectors

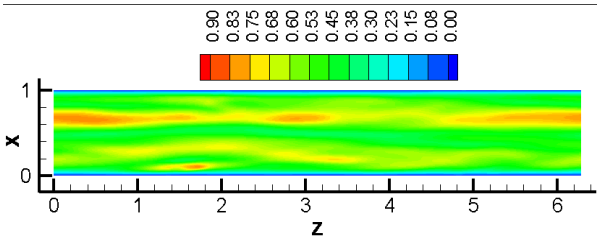

(Re=5978, Ha=21.2, 80x80x256)

Fig.6(c) Instantaneous velocity contours at y^+=8.85

Fig.7(a) and (b) shows the instantaneous and mean axial velocity superimposed with secondary velocity vectors at Ha=24.38. Laminarization is clearly seen at high Hartmann number with velocity flattening in the central, top and bottom regions. Secondary flows are completely dampened and flow becomes mainly dominated by flat axial velocity without any bulging in the corners. Velocity close to side-walls follows laminar hydrodynamic velocity profile. Fig. 7(c) gives instantaneous velocity plotted at y^+=8.85, with clearly showing laminarization along the length of the duct as well.

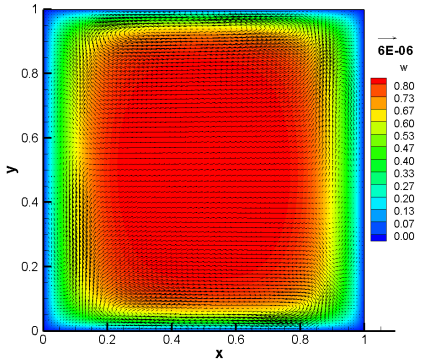

(Re=3350, Ha=24.38)

Fig.7(a) Instantaneous axial velocity contours with secondary velocity vectors

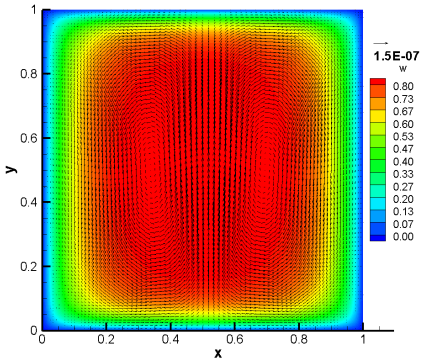

(Re=3350, Ha=24.38)

Fig.7(b) Mean axial velocity contours with secondary velocity vectors

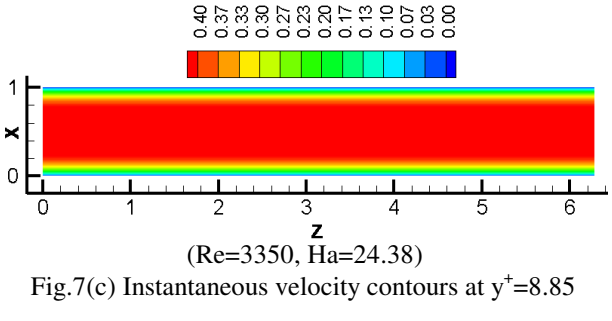

(Re=3350, Ha=24.38)

Fig.7(c) Instantaneous velocity contours at y^+=8.85

Fig. 8(a) shows the RMS of axial velocity fluctuations along horizontal bi-sector for various cases. As seen at low Hartmann numbers, RMS of velocity fluctuations close to side-walls is nearly the same as the non-magnetic case. Current simulation with Ha=21.2 and 80x80x256 mesh is found to match with Kobayashi's results close to the wall. However in the core of the duct, RMS fluctuations are much larger than reported by Kobayashi (22). For stronger magnetic field (Ha=22.26), turbulence is dampened close to side-walls but increases in the core. At further higher Hartman number (for example Ha=24.38), velocity fluctuations are completely dampened and the flow becomes laminar.

Fig-8(b) gives RMS of the axial velocity fluctuations along the vertical bi-sector for same cases. Close to top and bottom walls, because the magnetic field is perpendicular to the induced current, Lorentz force is strong and velocity fluctuations are damped even at lower Hartmann numbers. Velocity fluctuations at top and bottom walls are suppressed at lower Hartmann numbers than near side walls. Also, upon increasing the Hartmann number, velocity fluctuations are shifted from the wall region to the core of the duct before completely suppressed. However, turbulence close to side- and top-bottom walls is completely suppressed at around the same Hartmann number (~23). This finding is consistent with Kobayshi's (22) finding at moderate Reynolds number.

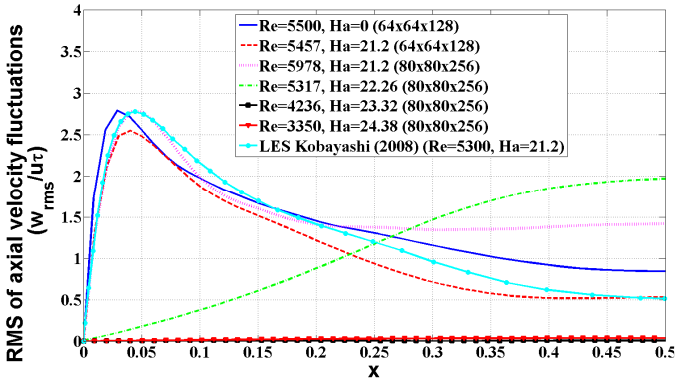

Fig-8 (a) RMS of axial velocity fluctuations along horizontal bisector

Fig-9(a), (b) and (c) gives the power spectrum of instantaneous velocity plotted as a function of wave number at the center, top-mid (0, 0.5D) and front-mid (0.5D, 0) locations at the cross-section of the duct based upon Taylor's frozen flow hypothesis (i.e. advection of turbulence is time independent) for Ha=21.2 case. Power spectrum in the inertial sub-range is found to be following -5/3 law at all three locations. This is consistent with Vorobev et al's work (26) for low magnetic interaction ($N = \frac{\sigma B_0^2 D_h}{\rho v}$ =~0.1, i.e. much smaller than 5) situations which is appropriate here.

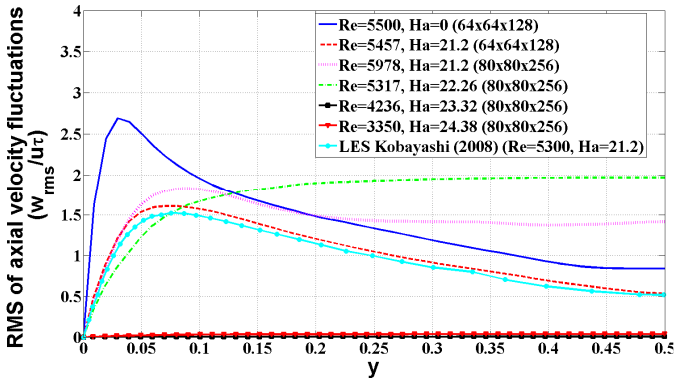

Fig-8 (b) RMS of axial velocity fluctuations along vertical bisector

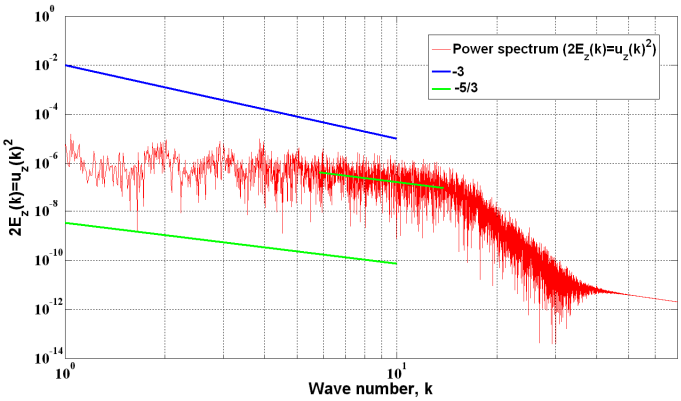

Fig-9(a) Power spectrum of instantaneous velocity (center)

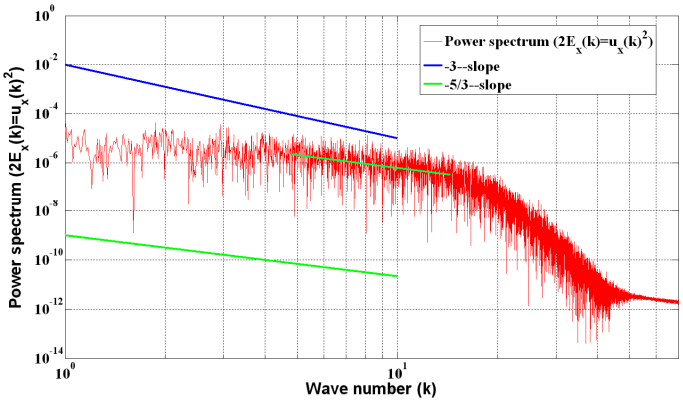

Fig-9(b) Power spectrum of instantaneous velocity (front-mid)

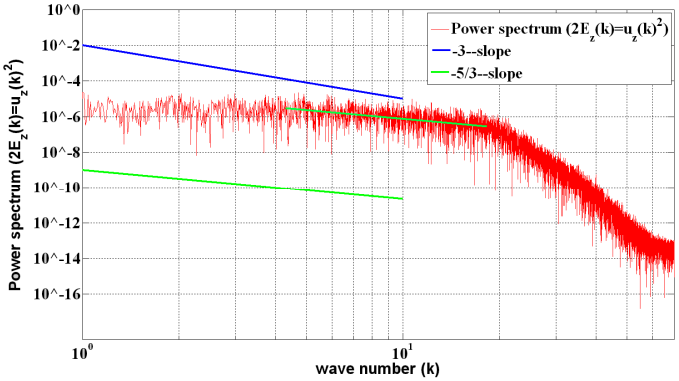

Fig-9(c) Power spectrum of instantaneous velocity (top-mid)

SUMMARY AND CONCLUSIONS

The present study has shown the effects of magnetic field on the turbulent flow development in a square duct at a nominal Reynolds number of 5500. The magnetic field is gradually varied from a low Hartmann number to a super-critical value when the flow becomes laminar. The grid used in the computations is fine enough that the simulations performed can be considered to be Direct Numerical Simulations (DNS). No sub-grid closure model has been included in the simulations. The simulations were performed by keeping a constant streamwise pressure gradient and varying the magnetic field. Thus the Reynolds numbers achieved decreased with increase of the magnetic field.

The magnetic field was found to suppress turbulence and flatten the velocity profile across the cross-section. Velocity flattening close to walls increases wall shear stress however turbulence suppression reduces it. Effect of these two phenomena is clearly seen in the case of Ha=21.2 case where Lorentz force assisted the pressure gradient and caused a higher flow rate. At higher Hartmann numbers (i.e. going from Ha=21.2 to Ha=22.26), velocity flattening takes over the suppression of turbulence and laminarization of the flattened velocity profile is seen to increase the friction factor from the minima. Power spectrum of instantaneous axial velocity at three selected locations is found to be following the -5/3 law. At Ha=21.2, maximum range of frequencies are reported at the front-mid location because the effect of the Lorentz force was not appreciable at this location for this Hartmann number.

ACKNOWLEDGMENTS

The authors gratefully thank Continuous Casting Consortium, Department of Mechanical Science & Engineering, University of Illinois at Urbana-Champaign, IL, for providing support for this work.

REFERENCES

(1) Davidson P. A., Magnetohydrodynamics in materials processing, Annu. Rev. Fluid Mech. 1999. 31:273–300

(2) Brian G. Thomas, Lifeng Zhang, Mathematical Modeling of Fluid Flow in Continuous Casting: a Review, ISIJ International, 2001, Vol.41, No.10, pp.1181-1193.

(3) R. Moreau. Magnetohydrodynamics. Kluwer Academic Publishers, 1990.

(4) Knaepen B. and Moreau R, Magnetohydrodynamic turbulence at low magnetic Reynolds number, Annu. Rev. Fluid Mech. 2008. 40:25-45.

(5) Ji HC, Gardner RA. 1997. Numerical analysis of turbulent pipe flow in a transverse magnetic field. *Int. J. Heat Mass Transf.* 40:1839–51

(6) Kenjereˇs S, Hanjali´c K. 2000. On the implementation of effects of Lorentz force in turbulence closure models. *Int. J. Heat Fluid Flow* 21:329–37

(7) Smolentsev S, Abdou M, Morley N, Ying A, Kunugi T. 2002. Application of the "K-ε" model to open channel flows in a magnetic field. *Int. J. Eng. Sci.* 40:693–711

(8) Smolentsev S, Moreau R. 2006. Modeling quasi-two-dimensional turbulence in MHD duct flows. *Proc. 2006 Summer Program*, pp. 419–30. Stanford, CA: Cent. Turbul. Res., Stanford Univ. & NASA Ames Res. Cent.

(9) Moin P. and Mahesh K., Direct Numerical Simulation: A Tool in Turbulence Research, Annu. Rev. Fluid Mech. 1998. 30:539-78.

(10) Kim, J., Moin, P. & Moser, R. 1987 Turbulence statistics in fully developed channel flow at low Reynolds number. *J. Fluid Mech.* 177, 133.

(11) Spalart, P. R. 1985 Numerical simulation of boundary layers. *NASA* TM88220-88222.

(12) Moser, R . D. & Moin, P., 1987 The effects of curvature in wall-bounded turbulent flows. *J. Fluid Mech.* 175, 479.

(13) Gavrilakis, S., 1992 Numerical simulation of low Reynolds number turbulent flow through a straight square duct. *J. Fluid Mech.* 244, 101.

(14) Huser Asmund and Biringen Sedat 1993, Direct numerical simulation of turbulent flow in a square duct, J. Fluid. Mech. Vol. 257, pp. 65-95.

(15) Ravi K. Madabhushi and S. P. Vanka, "Large eddy simulation of turbulence driven secondary flow in a square duct", Phys. Fluid A 3, 2734 (1991).

(16) Ravi K. Madabhushi and S. P. Vanka, “Direct numerical simulation of turbulent flow in a square duct at low Reynolds number”, Near-wall Turbulent flows, RMC So. C.G. Speziale and B. E. Launder (Editors) (1993).

(17) Satake Shin-ichi, Kunugi Tomoaki and Smolentsev Sergey, Direct numerical simulations of turbulent pipe flow in a transverse magnetic field, J. of Turbulence, 3 (2002) 020.

(18) Lee D and Choi H 2001 Magnetohydrodynamic turbulent flow in a channel at low magnetic Reynolds number *J. Fluid Mech.* 439 367–94.

(19) Satake Shin-ichi, Kunugi Tomoaki, Takase Kazuyuki and Ose Yasuo, Direct numerical simulation of turbulent channel flow under a uniform magnetic field for large-scale structures at high Reynolds number, Phy. Of Fluids 18, 2006.

(20) Zikanov Oleg and Thess Andre, Direct numerical simulation of forced MHD turbulence at low magnetic Reynolds number, J. Fluid Mech. (1998), vol. 358, pp. 299-333.

(21) Zikanov O. and Thess A., Direct numerical simulation as a tool for understanding MHD liquid metal turbulence, Appl. Mathematical Modelling 28, 2004 pp. 1-13.

(22) Kobayashi H., Large eddy simulation of magnetohydrodynamic turbulent duct flows, Phys. Fluids, 20 (2008).

(23) Batchelor, G. K., *An Introduction to Fluid Dynamics*, Cambridge University Press; ISBN:0521663962

(24) F. Harlow and E. Welch. Numerical calculation of time-dependenviscous incompressible flow of fluid with free surface. *Physics of Fluids*,8:2182-2189, 1965.

(25) U. Muller and L. Buhler, Magneto Fluid Dynamics in Channels and Containers (Springer, Berlin, 2001), Sec. 4.2.1.

(26) Vorobev A., Zikanov O., Davidson P. A. and Knaepen B., Anistropy of magnetohydrodynamic turbulence at low magnetic Reynolds number, Phys. Fluids 17, (2005).